NAVAL POSTGRADUATE SCHOOL

MONTEREY, CALIFORNIA

THESIS

MODELING A 400-HZ SIGNAL TRANSMISSION
THROUGH THE SOUTH CHINA SEA BASIN

by

Chris S. Bernotavicius

March 2009

Thesis Co-Advisors: Ching-Sang Chiu
                                                       Clyde Scandrett

Approved for public release; distribution is unlimited

THIS PAGE INTENTIONALLY LEFT BLANK

13. ABSTRACT (maximum 200 words)

As part of the Office of Naval Research (ONR) sponsored Windy Island Soliton Experiment (WISE), two deep water moorings were placed in the northeastern portion of the South China Sea deep basin to conduct an acoustic propagation study. For approximately one year the source and receiver transmitted and received phase-modulated signals to measure the multi-scale variability in the transmission loss induced by the ocean mesoscale variability and the progression of internal tides and waves. A numerical acoustic propagation model based on Hamiltonian ray tracing is utilized to replicate the observed basic arrival structure and transmission loss. Being able to accurately model the basic arrival structure is a necessary first step before modeling the observed variability can be attempted. The comparison of the modeled arrival structure with the actual data was utilized to refine the angular resolution of the ray fan in the model, estimate the geo-acoustic properties of the bottom, and develop transmission loss estimates. Transmission loss measurements from sono-buoy data were used as an independent metric to evaluate the model.

THIS PAGE INTENTIONALLY LEFT BLANK

MODELING A 400 HZ SIGNAL TRANSMISSION THROUGH THE SOUTH CHINA SEA BASIN

Chris S. Bernotavicius
Lieutenant, United States Navy
B.S., Pennsylvania State University, 2002

Submitted in partial fulfillment of the
requirements for the degree of

MASTER OF SCIENCE IN APPLIED MATHEMATICS

from the

NAVAL POSTGRADUATE SCHOOL
March 2009

Author: Chris S. Bernotavicius

Approved by: Ching-Sang Chiu
                Thesis Advisor

                Clyde Scandrett
                Thesis Advisor

                Carlos Borges
                Chairman, Department of Mathematics

THIS PAGE INTENTIONALLY LEFT BLANK

ABSTRACT

As part of the Office of Naval Research (ONR) sponsored Windy Island Soliton Experiment (WISE), two deep water moorings were placed in the northeastern portion of the South China Sea deep basin to conduct an acoustic propagation study. For approximately one year the source and receiver transmitted and received phase-modulated signals to measure the multi-scale variability in the transmission loss induced by the ocean mesoscale variability and the progression of internal tides and waves. A numerical acoustic propagation model based on Hamiltonian ray tracing is utilized to replicate the observed basic arrival structure and transmission loss. Being able to accurately model the basic arrival structure is a necessary first step before modeling the observed variability can be attempted. The comparison of the modeled arrival structure with the actual data was utilized to refine the angular resolution of the ray fan in the model, estimate the geo-acoustic properties of the bottom, and develop transmission loss estimates. Transmission loss measurements from sono-buoy data were used as an independent metric to evaluate the model.

THIS PAGE INTENTIONALLY LEFT BLANK

TABLE OF CONTENTS

LIST OF FIGURES

THIS PAGE INTENTIONALLY LEFT BLANK

LIST OF TABLES

THIS PAGE INTENTIONALLY LEFT BLANK

ACKNOWLEDGMENTS

Heartfelt thanks is extended to both of my advisors, Professor C. S. Chiu of the Oceanography Department and Professor C. Scandrett of the Math Department. I appreciate their in-depth reading and comments. A thanks is also due to research associate Chris Miller who helped in numerous ways with the data and analysis. Finally, thanks to my wife for supporting me.

THIS PAGE INTENTIONALLY LEFT BLANK

I.   INTRODUCTION

A.   SOUTH CHINA SEA OCEANOGRAPHY AND GEOMETRY

The South China Sea (SCS) is a marginal sea located in the western Pacific Ocean. It consists of a deep basin surrounded by a shallow continental shelf to the north and west, and tropical islands to the south. The deep basin portion is located in the eastern central portion of the SCS and reaches depths in excess of 4,000 meters. The SCS is connected to other seas and the north Pacific through a variety of straits, the most significant of which is the Luzon strait, which provides the great majority of mass transport into the SCS (Ramp et al. 2004).

The SCS is home to significant environmental variability on scales ranging from the super-tidal to seasonal, which consequently induces variability in the SCS acoustic propagation. Some of the more interesting features include variable wind forcing, intrusion of the Kuroshio current, and large internal waves. The SCS wind forcing features summer and winter monsoon seasons, as well as tropical cyclones. The Kuroshio current is the strong western boundary current of the northwestern Pacific ocean. It has been observed to enter the SCS via the Luzon strait, and its subsequent behavior is widely variable. Possible scenarios include bifurcation, simply exiting (meander), or forming a warm core ring that can propagate across the SCS. (Ramp et al. 2004) Finally, the SCS features large internal waves that appear to be generated in the Luzon strait via the abrupt topography change. These non-linear waves are among the largest observed and can impact the sound speed profile and, thus the acoustic propagation in the basin. One of the major goals of the Windy Island Soliton Experiment (WISE) was to study the impact of the internal waves on acoustic propagation.

B.   WISE EXPERIMENT OVERVIEW

The Windy Island Soliton Experiment (WISE) represents a collaborative effort between Taiwan and US researchers to study the formation and evolution of the trans-basin, non-linear internal waves in the Northeastern South China Sea. Moorings were placed on the continental shelf, the deep basin, and in the Luzon Strait for a period of a

year commencing in April 2005. In addition to this main focus, two acoustic propagation studies were conducted, one over the shallow continental shelf, and one in the deep basin in order to study the physics of sound propagation in the SCS environment, and the impact of the large internal waves on sound transmission. In particular, the focus of the basin study was to characterize the impact of the trans-basin internal waves on long-range transmission loss. Physically, this was accomplished by utilizing two deep-water moorings that transmitted and received a phase modulated 400 Hz signal repeatedly for a period of a year. The processed signal (the output of a correlation-matched filter) corresponds to the multipath arrival structure of a pulse. The modeling of the observed basic arrival structure and transmission loss in a "mean ocean" is the focus of this thesis.

C.   NAVAL RELEVANCE

The Naval relevance of this thesis takes two distinct forms. The SCS is area of significant tactical importance to the Navy, and is home to major shipping lanes that account for a significant portion of world commerce. This study investigates the observed acoustic arrival structure in the SCS basin, hopefully, eventually leading to an improved understanding of acoustic propagation in this body of water. Follow-on studies will focus on attempting to understand the acoustic variability as a function of trans-basin internal waves, which will provide valuable information for potential operations. In addition, this study examines the geo-acoustic properties of the SCS bottom, valuable information for operational planning and modeling.

D.   APPROACH

The overall objective of this thesis is to develop and refine a numerical model of the 400 Hz signal transmission, in particular the basic arrival structure at the receiver and the transmission loss as a function of range along the path. Development of an accurate model of the basic arrival structure and transmission loss for the acoustic path used in the study will permit future modeling study on the impact of the trans-basin internal waves on sound transmission variability. The numerical model is based on Hamiltonian Ray tracing, the numerical integration of Hamilton's equations as described in (Georges, Jones, & Riley, 1986) and (Chiu, Semtner, Ort, Miller, & Ehret, 1994). Known

environmental data includes accurate bathymetry and a mean sound speed profile determined through Conductivity-Temperature-Depth (CTD) casts taken during the WISE experiment. There are three primary modeling focuses in this effort. The first is an empirical determination of the necessary angular resolution for the ray fan. Equivalently, over a given angular span what is the initial ray density required to accurately model the observed data. The second focus is the estimation of the geo-acoustic properties of the sediment, a requirement for accurate modeling of the amplitudes of the multi-path arrivals. The final focus is the development of a transmission loss curve and the comparison with independent measurements as an evaluator of the model.

E.   THESIS OUTLINE

The remainder of this thesis consists of three chapters, Chapter II – Methodology, Chapter III – Modeling and Data Comparison, and Chapter IV – Results and Conclusions. An appendix containing derivations of some equations is also included. Chapter II discusses the WISE experiment and the data collected in more detail along with Hamiltonian Ray tracing and the Hamiltonian Acoustic Ray-tracing Program for the Ocean (HARPO) model, described in (Georges, Jones, & Riley, 1986), as well as the approach utilized in this thesis to synthesize the arrival structure. Chapter III contains the modeling results and their comparison with actual data. Chapter IV provides a summary of significant results.

THIS PAGE INTENTIONALLY LEFT BLANK

II.   METHODOLOGY

A.   WISE TECHNICAL PARAMETERS AND DATA

1.   Basin Experiment

The basin acoustic study portion of the WISE experiment consisted primarily of a transmitter and receiver moored approximately 167 km apart with the source and receiver at a depth of approximately 840 m. The general arrangement is depicted on Figure 1, where the locations of the transmitter and receiver are designated as B2 and B1 respectively. Additional sono-bouy measurements were taken between B2 and B1 to measure transmission loss; these measurements were not used in the modeling effort, but rather reserved as an independent evaluation of the transmission loss predictions.

The sound source was a 400 Hz source that transmitted a 5.11 s, 511 digit pseudo-random signal at $\sim 183\,dB$ re 1 μPa at 1 m, with a bandwidth of 100 Hz. The source itself consisted of a six m array of four hydrophones. Signal processing gain was achieved by pulse compression along with coherent averaging the eight m-sequence cycles per separate reception. The final signal processing gain for an individual hydrophone was:

$$10\log_{10}(8) + 10\log_{10}(511) = 36.1 \text{ dB}$$

The desire to sample the internal waves in the basin, along with hardware considerations dictated a transmission period of 15 minutes. The moorings were recovered; the batteries were serviced and redeployed a number of times throughout the year. The locations and transmitter/receiver information used are from the final such deployment. Full technical details of the entire basin experiment are available in provided in (Miller et al. 2009)
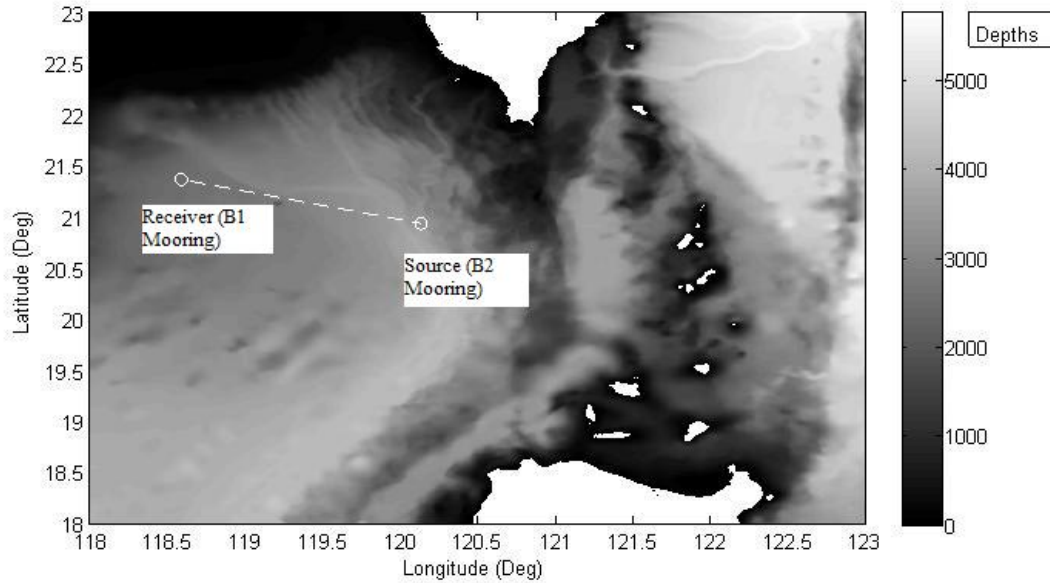
Figure 1.   **Locations of the source (B2) and receiver (B1) in the SCS superimposed on the bathymetry.**

2.   Data Collected

For each reception, the demodulated, coherent averaged data was saved for each of the hydrophones. The data that was utilized in this study consisted primarily of coherent averaged acoustic arrival structures that have been corrected for mooring motion (Chiu et al., 2008). Some examples of the observed arrival structures are shown in Figure 2. It is clear that the long timeframe of this experiment admits a large degree of variability into the individual arrival structures, and indeed the magnitude of the first peak varies significantly, as can be seen from Figure 2. While the intensity of the individual peaks in the arrival varies significantly, the basic structure itself, which is comprised of a large arrival followed by a number of smaller arrivals, is fairly consistent. Five significant peaks were consistently observed for the duration of the WISE experiment, as is evident from Figure 3. Temporal variability is clearly present, which is not the subject of this thesis. Modeling the basic arrival structure then is the goal of this thesis, along with a reasonable approximation of the mean intensity.
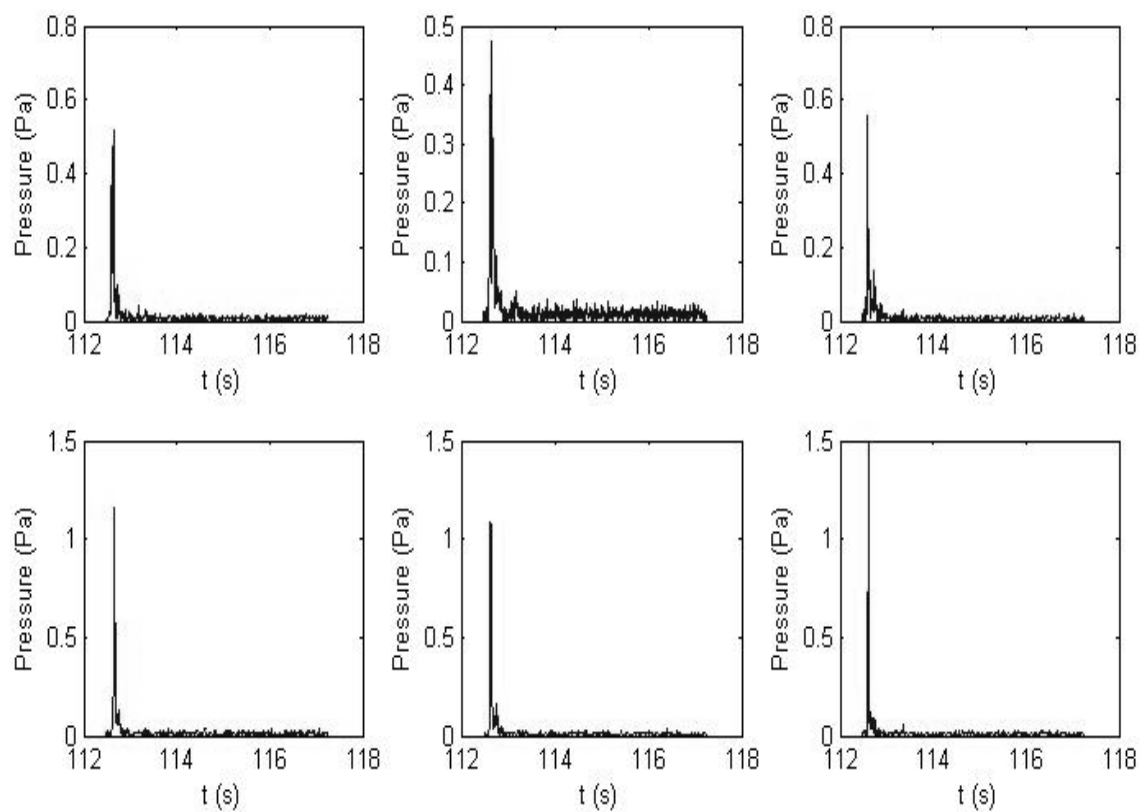
Figure 2.   Six samples of acoustic arrival structures observed between June and October 2006.

7
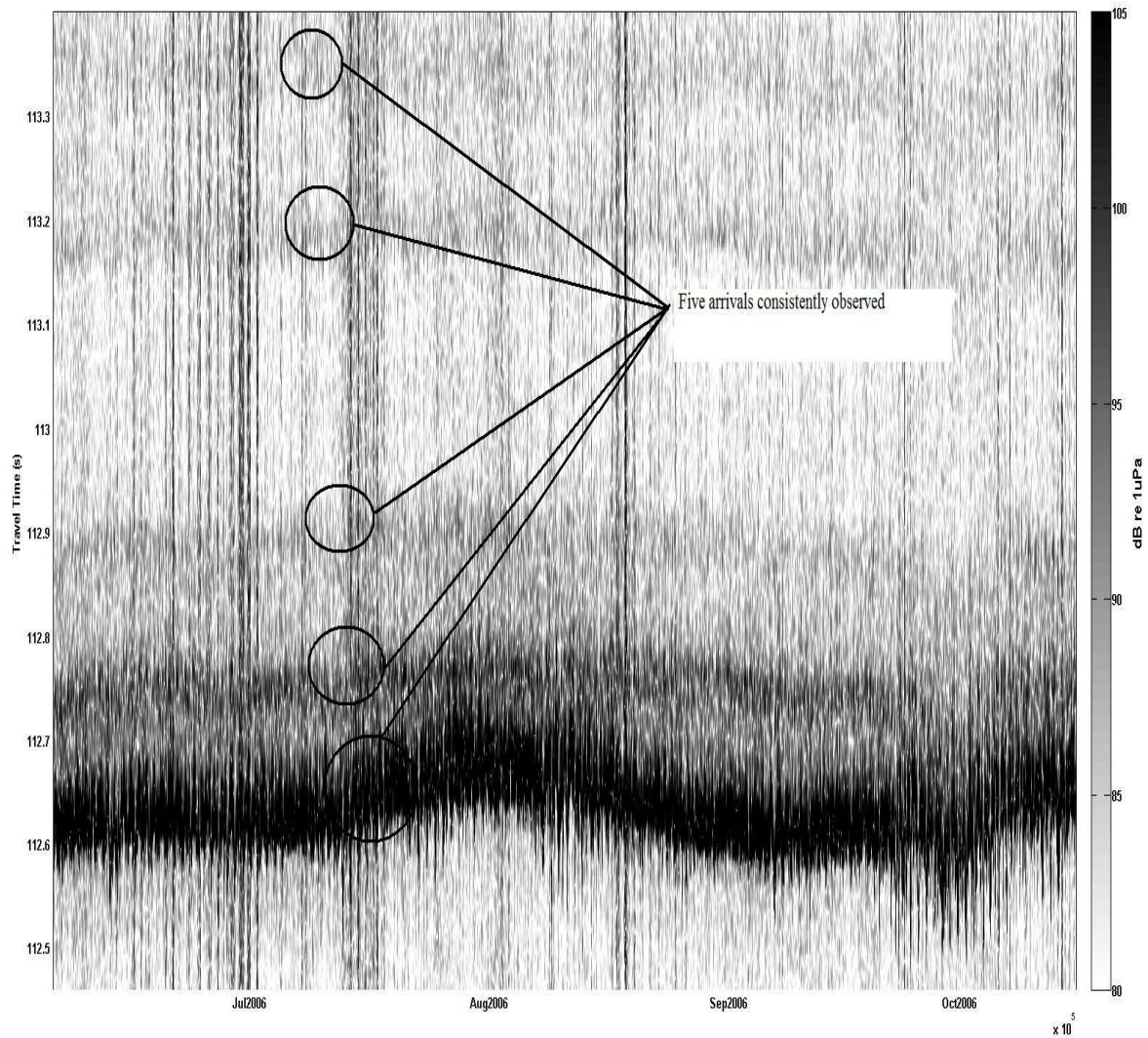
Figure 3. The observed arrival structure as a function of transmission time – displayed in dB re 1 μ Pa to highlight the later weak arrivals. (from Chiu et al., 2008)

B. RAY THEORY AND HAMILTONIAN RAY TRACING

1. General Ray Theory and the Eikonal Approximation

In general, modeling acoustic propagation through the ocean necessitates solving the governing wave equation:

$$\nabla^2 p - \frac{1}{c(\vec{r})^2} \frac{\partial^2 p}{\partial t^2} = 0 \tag{2.1}$$

Where p represents pressure, c is the sound speed, t denoted time, and $\vec{r}$ is a vector representing position. In ray acoustics the assumption is made that the environmental change and thus the variation in sound speed is gradual over a small number of acoustic wavelengths. Ray acoustics involves the further assumption that solutions of this equation are of the form:

$$p(\vec{r},t) = A(\vec{r}) \exp(i[2\pi f t - k_0 W(\vec{r})]) \tag{2.2}$$

Where $k_0 = \dfrac{2\pi f}{c_0}$ is the reference wave number, and $W(\vec{r})$ is the *eikonal* and represents the phase component of the solution. Since solutions of constant phase represent wave fronts, and rays travel in a direction orthogonal to the wave front, this assumption leads to a relation that governs the ray paths. The ray equations are given below; the eikonal equation yields the ray equations and the ray paths while the transport equation provides ray amplitudes. Here the ratio of sound speed to a reference sound speed $\left(\frac{c_0}{c(\vec{r})}\right)$ is given as the dimensionless quantity n, referred to as the index of refraction, and s is the distance along the ray.

$$\begin{aligned}
&\text{Eikonal Equation:} \quad \left|\nabla W(\vec{r})\right|^2 = n(\vec{r})^2 \\
&\text{Transport Equation:} \quad 2\nabla A(\vec{r}) \cdot \nabla W(\vec{r}) + A(\vec{r})\nabla^2 W(\vec{r}) = 0 \\
&\text{Ray Equations:} \quad \frac{d}{ds}\left(n(\vec{r})\frac{d\vec{r}}{ds}\right) = \nabla n(\vec{r})
\end{aligned} \tag{2.3}$$

A full derivation of these equations and the resultant ray equations can be found in the Appendix or in a reference such as (Ziomek 1995). The ray approximation is also known as the low gradient approximation since it requires:

$$\left|\frac{\nabla^2 A(\vec{r})}{k_o^2 A(\vec{r})}\right| \ll 1 \Leftrightarrow 2\pi f \gg |\nabla c| \tag{2.4}$$

9

For a transmission frequency of 400 Hz the quantity $2\pi f$ is at least four orders of magnitude larger than $|\nabla c|$. The ray paths can be obtained numerically by integrating Hamilton's equations, which are equivalent to the ray equations shown above, but derived in an alternative fashion from variational principles.

2. Hamiltonian Ray Tracing

Hamilton's equations for a static (no current) ocean are given as:

$$\frac{d\vec{r}}{d\tau} = \nabla_k H(\vec{r},\vec{k})$$

$$\frac{d\vec{k}}{d\tau} = -\nabla H(\vec{r},\vec{k})$$

$$\text{with } H(\vec{r},\vec{k}) \equiv (2\pi f)^2 - c(\vec{r})^2 \left|k^2\right|$$

$$\text{and } \tau = \frac{-t}{4\pi f}$$

(2.5)

Where t represents travel time and τ is used for the dependent variable in Hamilton's equations. The equivalence is based on a variational theme. The rays travel perpendicular to the wave fronts and they travel along the path of shortest time subject to the constraint of the index of refraction. The integration of Hamilton's equations with a suitably defined Hamiltonian gives just such variational paths. An interesting derivation that uses only elementary differential operations can be found in (Molcho and Censor 1986). An overall view of the topic, which has its origins in geometrical optics, can be found in (Cornbleet 1983) where Hamilton's approach and the eikonal approximation are compared. A discussion of the Hamiltonian as a dispersion relation and the actual equations integrated is given in the Appendix.

3. Numerical Integration

This approach reduces the solution of the free wave equation on some section of the ocean to an initial value problem – integrating a set of first order ODE's. The initial conditions specified are the ray launch angles. The HARPO code in FORTRAN originated from the NOAA Wave Propagation Laboratory described in (Jones, Riley and Georges 1986) It integrates Hamilton's equations in three dimensions in polar spherical

10

coordinates. HARPO utilizes the Adams-Moulton predictor corrector for the numerical integration, with a Runge-Kutta starter. The starter is also used at each boundary interaction and turning point. The algorithm initially sets the wave number $\vec{k}$ equal to the value expected by the dispersion relation, that is $\left|\vec{k}\right|^2 = \dfrac{(2\pi f)^2}{c^2(\vec{r})}$; $\vec{k}$ is then allowed to vary freely as Hamilton's equations are integrated. The error is then evaluated by setting

$$Error = \frac{\left|\vec{k}\right|^2}{\left|\vec{k}\right|^2_{disp}} - 1, \text{ where } \vec{k}_{disp} \text{ is the wavenumber expected from the dispersion relation.}$$

The Runge-Kutta (RK) algorithm is utilized to provide four initial points to start the Adams-Moulton (AM) integration step. At the conclusion of each AM integration the error is checked against a user provided maximum error. If the error has been exceeded, the step size is reduced and the process begins again with the RK step.   This approach has the advantage of some numerical efficiency as the Adams-Moulton method is an implicit, multi-step method (of $O(h^5)$) that varies the step size based upon the error, which is related to the gradient. When the gradient is high, the step size will be low and the problem will be more computationally complex. When the gradient is low, as in this modeling effort, the step size can be large. Full details of the particular integrating algorithms implemented and the associated errors can be found in (Jones, Riley and Georges 1986).

4.   Detecting Bottom and Surface Interactions

HARPO requires bottom data that is continuous and smooth enough to preclude very irregular shapes where diffraction is important and detection of bottom interactions can be very difficult. HARPO handles bottom and surface interactions in three steps. First, a bottom interaction is noted at some integration step by observing that a surface (discontinuity in the index of refraction) has been crossed. HARPO then iterates backwards until the surface is reached, and finally computes a reflection direction and then begins integrating in the new direction.

11

C.   THE HARPO MODEL

1.   Inputs and Technical Data

The original HARPO model described in (Georges, Jones and Riley 1986) handled only canonical oceans and boundary conditions. The code was modified significantly by (Chiu et al. 1994) to permit the use of gridded data via empirical orthogonal eigenfunction decomposition. Bi-cubic splines are fit through the gridded data to create continuous representations of the bottom and sound speed field. This revision also created MATLAB code that interfaces with HARPO for ray set analysis, eigenray search, and arrival structure synthesis.

The HARPO model is fully three dimensional and can support three dimensional sound speed data. The gridded bathymetry and sound speed data, along with the source-receiver geometry are the required data inputs. The ray launch angles are the initial conditions.

2.   Ray Set Output

The output of the HARPO model is a text file that defines the ray geometry. It provides the ray coordinates in spherical polar coordinates referenced to the mean sea level. This of course can be imported into a program such as MATLAB and can provide a graphical representation of the ray paths. This however does not provide an arrival structure or any method to determine which rays interact with the receiver. Additionally, the ray set provides turning points and interaction with the surface and bottom. This permits subsequent analysis to consider the impact of bottom interaction on the energy transmitted along the ray path. What follows describes the methodology of the code developed and described in (Chiu, Semtner, Ort, Miller, & Ehret, 1994).

D.   RAYSET ANALYSIS

1.   Ray Amplitude Determination

There are two primary factors that must be accounted for to determine ray amplitude. The first is the loss of energy as the ray travels through the ocean. In ray acoustics this is modeled via ray tube spreading, the concept that as a ray tube (bundle of

rays) travels through the ocean no energy is lost through the sides of the tube since the rays are perpendicular to wave fronts. As the rays travel through the ocean, the perpendicular area at the end of a ray tube spreads or contracts, resulting in a different cross sectional area, and thus a varied intensity. This quantity is inversely proportional to the change in ray range with respect to the change in launch angle for a fixed depth and can be shown to be:

$$p^2 = p_0{}^2 \frac{R_0}{r} \frac{c}{c_0} \left| \frac{\cos\theta_0}{\cos\theta} \right| \frac{1}{\left| \dfrac{dz}{R_0 d\theta_0} \right|_r} \tag{2.6}$$

Where p is pressure, r is range θ_0, θ are the initial launch angle and the ray angle at range r respectively. R_0 represents the reference range (1 m) and c_0 the sound speed at reference range. The MATLAB code of (Chiu, Semtner, Ort, Miller, & Ehret, 1994) is utilized to compute this derivative numerically via finite differences using adjacent rays. The code utilizes first order centered differences with the exception of the rays located at the edges of the angular span. For these rays first order forward and backward differences are used. When the derivative vanishes (indicating a caustic) or the ray angle becomes a multiple of $\dfrac{\pi}{2}$, the code moves outward to the next set of adjacent rays. This

allows the code to track through caustics, but emphasizes the need to select a fine enough angular resolution to obtain a convergent representation of the ray amplitude.

The second factor is the loss in ray amplitude due to an interaction with the bottom or surface. The approach utilized here is that of (Clay and Medwin 1977), where the interaction with the bottom is simulated as a reflection of a lossy half space. A full derivation of the equations given below is located in the aforementioned reference. The loss is accounted for by considering the grazing angle of the ray when it hits the bottom θ_1, the water column sound speed c_1, the sediment sound speed c_2, and the density of the water column and bottom ρ_1, ρ_2. The attenuation of compression waves in the bottom sediment is parameterized by letting the sound speed in the sediment be a complex quantity with:

13

$$Im(c_2) = \frac{c_2{}^2}{2\pi f} \frac{\alpha f}{1000} \frac{1}{20\log_{10} e} \qquad (2.7)$$

This, combined with the assumption of a plane wave solution yields the following reflection coefficient.

$$\Re_{12} = \frac{\rho_2 \operatorname{Re}(c_2)\sin\theta_1 + i\rho_2 \operatorname{Im}(c_2)\sin\theta_1 - \rho_1 c_1 \sin\theta_2}{\rho_2 \operatorname{Re}(c_2)\sin\theta_1 + i\rho_2 \operatorname{Im}(c_2)\sin\theta_1 + \rho_1 c_1 \sin\theta_2} \qquad (2.8)$$

Where θ_2 is determined from Snell's law:

$$\theta_2 = \arccos[\frac{\operatorname{Re}(c_2) + i\operatorname{Im}(c_2)}{c_1}\cos\theta_1] \qquad (2.9)$$

The MATLAB code of (Chiu, Semtner, Ort, Miller, & Ehret, 1994) is utilized to track the ray amplitude through each interaction with the bottom and surface.

2.   **Eigenray Search & Parameters**

In order to model the multipath acoustic arrival structure it is first necessary to identify the acoustic paths between the source and the receiver, the so-called eigenrays. The MATLAB code of Chiu, Semtner, Ort, Miller, & Ehret, 1994) utilized to search the ray set and determine the eigenray parameters. The code determines the depth difference at the receiver range between the ray and the receiver for each ray as a function of launch angle, θ_0. By finding the zeroes of this curve, or the places where the depth difference is zero, the precise eigenray parameters can be obtained. The eigenray determination does not involve retracing any rays – for the purpose of plotting eigenrays, those rays nearest the eigenrays are utilized. A sample of this curve is shown to illustrate the process in Figure. 4. The MATLAB code is also used to determine the eigenray parameters such as amplitude a_n , phase ϕ_n , and phase front arrival time t_n .
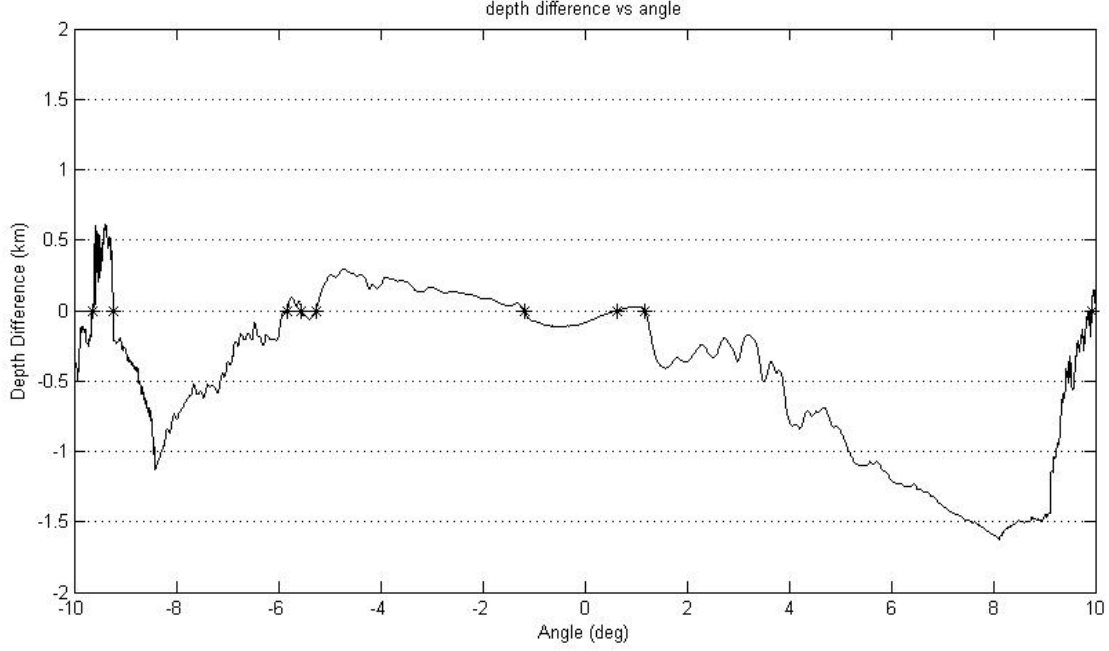
Figure 4. **A curve is fit through the depth difference vs. launch angle for each ray – the zeroes of this curve represent eigenrays (shown as stars) and permit the eigenray parameters to be precisely determined.**

3. Generating Acoustic Arrival Structure

Once the eigenray parameters have been determined, an acoustic arrival structure can be generated via the following equation. A model pulse is created to match the energy and shape of the output of the correlated match filter used in signal processing. A comparison of these two pulses is shown in Figure 5. Given this pulse, and the eigenray parameters identified above, the resultant acoustic arrival structure can be expressed as:

$$\tilde{r}(t) = \sum_{eigenrays} a_n \tilde{s}(t - t_n) \exp[-i(2\pi f_o t_n + \phi_n)] \tag{2.10}$$

Where the $\tilde{r}, \tilde{s}$ indicated the complex envelope at the receiver and source respectively. A discussion of this approximation can be found in (Hager 2008).

15
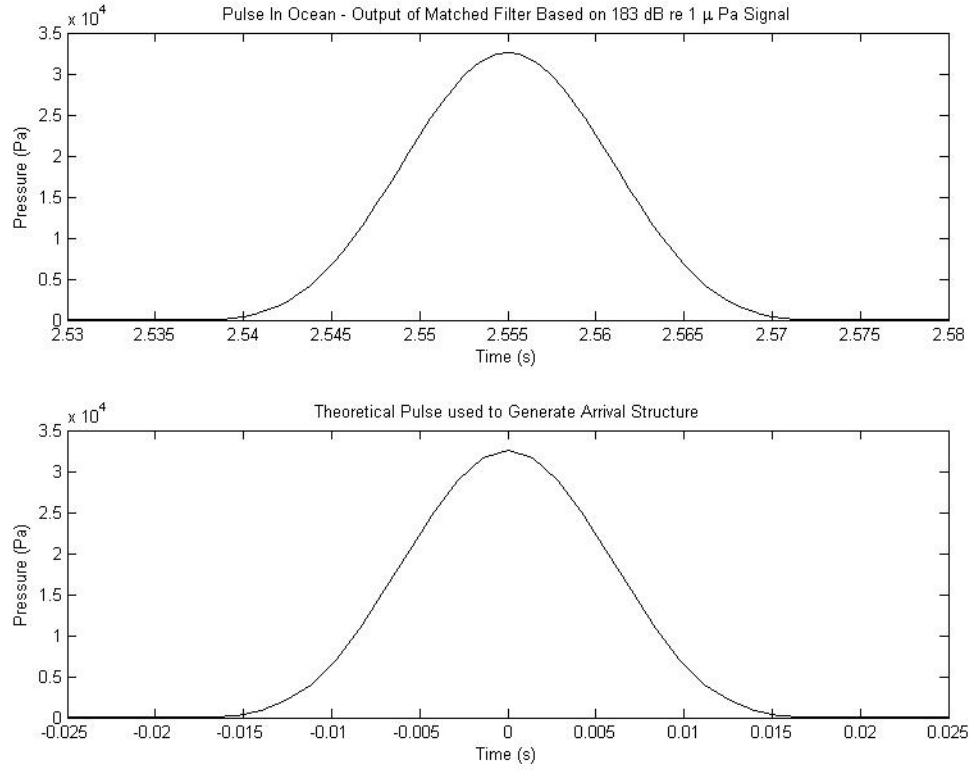
Figure 5. **A comparison of the theoretical pulse used to synthesize the arrival structure and the output of the correlated match filter.**

4. Modeling Methodology

The next chapter details the application of this methodology to the specific goals of this thesis. First, the acoustic arrival structure is generated at increasingly refined angular resolutions to determine what resolution is necessary to obtain a convergent arrival structure while minimizing the computational intensity of the problem. Once such a satisfactory ray set is obtained the geo-acoustic parameters of the bottom are tuned to match the structure of the arrival to the observed data. Finally, transmission loss predictions are generated and compared to independent data obtained by sonobuoys during the WISE experiment.

III.   MODELING AND DATA COMPARISON

A.   BATHYMETRY AND SOUND SPEED DATA

1.   Bathymetry

The two sets of gridded data required by the model are the bathymetry and the sound speed profile. The bathymetry utilized was extracted from a high resolution transect from the Luzon Strait courtesy of (Liu et al. 1998). The input data is referenced from the location of the source (B2) and reflects the deep basin nature of the problem with only some gentle shoaling. Some smoothing was utilized to prevent the discrete nature of the data from introducing erratic or chaotic behavior in the ray paths. Figure 6 shows a graphic representation of the bathymetry with the source and receiver annotated.
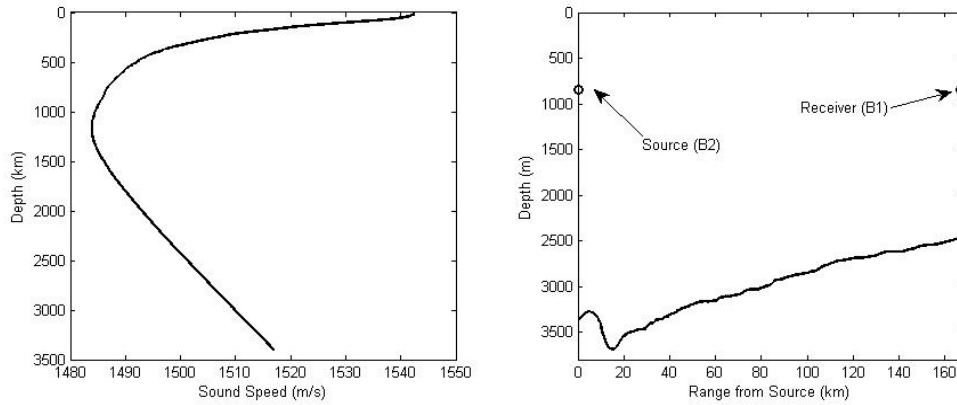
Figure 6.   Gridded data input to HARPO, the sound speed profile shown in the left pane is a mean of CTD casts taken during the WISE experiment and the bathymetry shown in the right pane is that between the source and receiver.

2.   Sound Speed Profile

In this modeling effort, a single sound speed profile (SSP) was utilized to create a range independent sound speed field. This profile represents the mean of the CTD casts taken during the WISE experiment. The location of the source and receiver in the SSP indicates that both refracted-refracted rays and bottom interacting rays should be expected.   Figure 7 shows that most of the rays interact with the bottom many times,

17

making the bottom composition an item of key importance in modeling the arrival structure. Some smoothing was conducted on the gridded data, as well as extrapolating the profile in the gridded data set to ensure that it extended to the bottom at all ranges – ensuring continuity and smoothness of the bottom and sound speed representations.

3.   Coordinate System

The actual latitude/longitude coordinate system is translated to a simple model coordinate system where the rays can be shot due north. The ranges and curvature of the actual coordinate system are preserved. The HARPO model is fully capable of the complexities of a three dimensional, range-dependent problem, the focus of this effort, however, was to model the basic arrival structure in a geometry that consisted of a source and receiver in line with each other. Therefore, the range independent sound speed profile and the bathymetry were duplicated to create a three-dimensional box where the rays will behave in a two dimensional fashion.
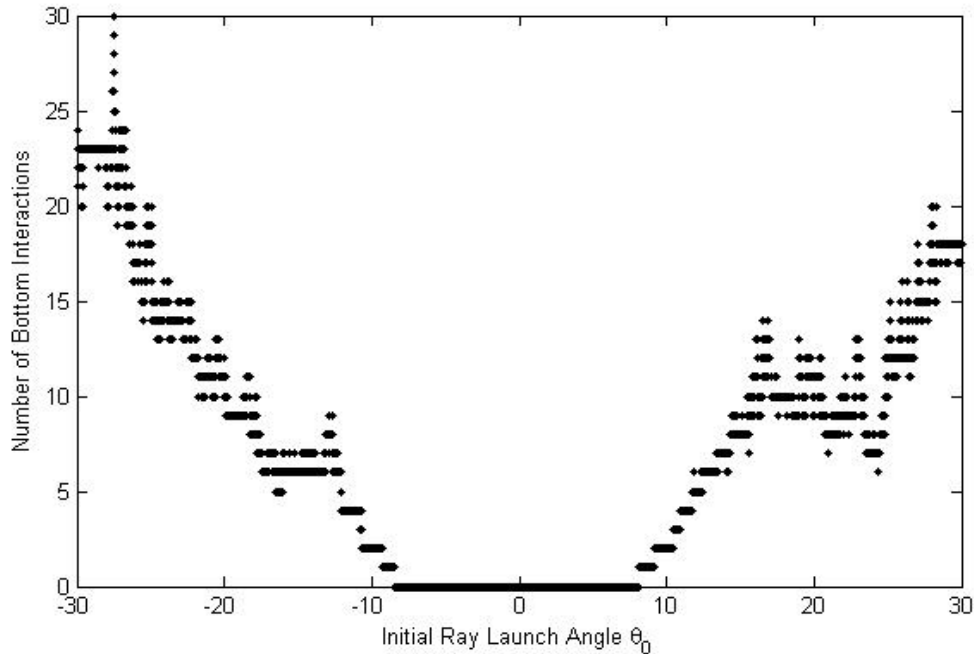
Figure 7.   The dependence of the number of bottom interactions on launch angle – showing the large majority of rays in the ray fan interact with the bottom many times.

18

B. ANGULAR RESOLUTION STUDY

1. Angular Aperture

It is desirable to study the angular resolution to ensure that no possible eigenpaths are missed, and the modeled arrival structure converges in amplitude. At the same time, over a fixed angular aperture an increase in resolution requires a larger number of rays to be traced which in turn increases the computational requirements. It is desirable then to minimize the total angular aperture. It is true that there is a critical angle θ_o, beyond which total internal reflection occurs – but this is a function of the bottom and since a priori we cannot be certain of the bottom, we must select an angular aperture which will contain the critical angles for all reasonable bottom choices. The geo-acoustic properties of the bottom and the characterization of the bottom in this effort are discussed in a later section. To ensure that the critical angles of all possible bottoms were included it was necessary to utilize an aperture of at least $[-20^o, 20^o]$. Figure 7 additionally shows that rays outside this window interact with the bottom many times, greater than ten, and thus could not contribute to the arrival structure in a significant way.

2. Angular Resolution

A set of modeled arrival structures resulting from a progressive refinement in angular resolution is shown in Figure 8. The angular resolution impacts the convergence of the arrival structure in two ways. First, it is necessary to ensure that all contributing eigenpaths are captured. Figure 8 shows that the structure is fairly constant with a resolution as course as 0.05^o, indicating that at this resolution all contributing eigenpaths have been captured. The second concern is convergence in amplitude. Since the ray tube spreading is approximated with finite differences, it is necessary to utilize an angular resolution fine enough to obtain a sufficiently convergent representation of ray amplitude. It can be seen from Figure 8 that the amplitude converges at the finer resolution of $0.01^o / 0.005^o$. Further refinements $(0.0025^o / 0.001^o)$ confirmed these results. The bottom utilized in this depiction is the one that was ultimately selected as the best match:

19

a silty-clay bottom whose properties are discussed below. At these resolutions, the five arrivals that were consistently observed during the WISE effort (Figure 3) are clearly observable.
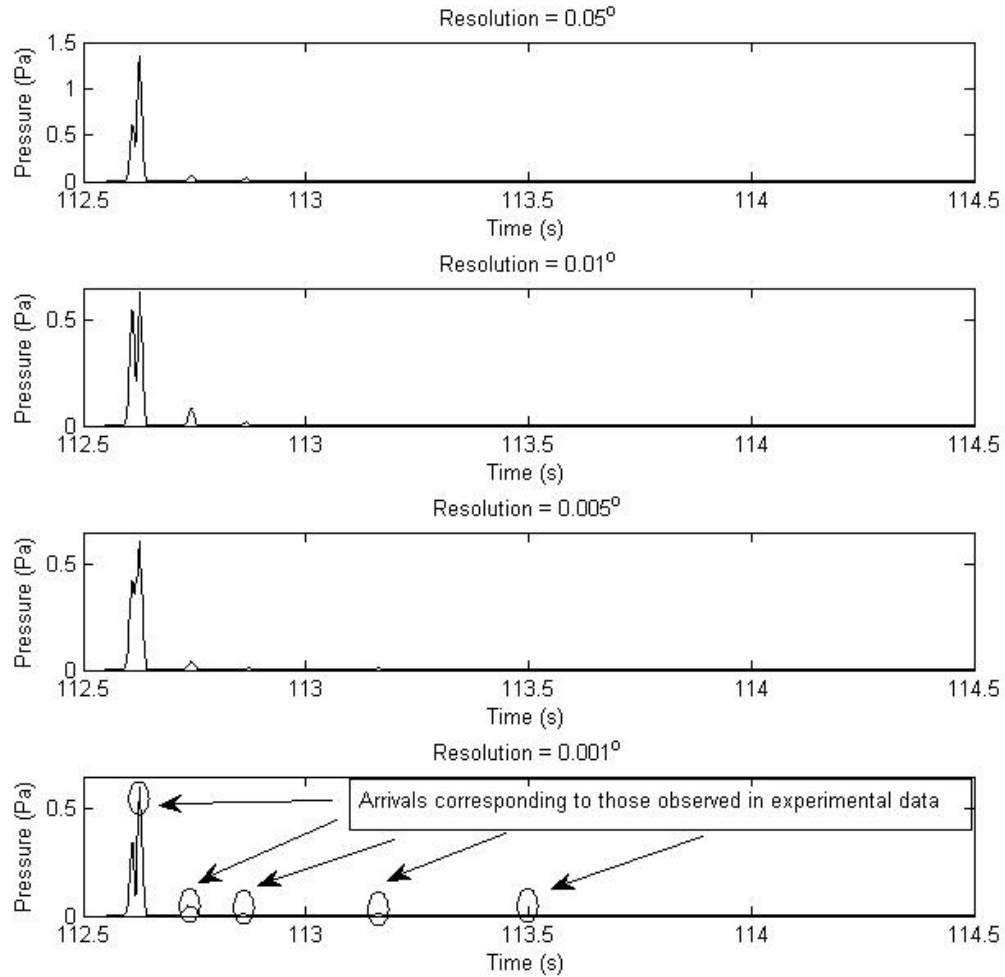
Figure 8. **Modeled arrival structures corresponding to a refinement in angular resolution; the structure is stable at 0.05^o, but convergence in amplitude requires a finer resolution.**

3. Eigenray Composition

The eigenray composition of each of the five observable arrival pulses is shown in Figure 9. The first arrival occurs at approximately 112.6 seconds and is comprised

entirely of refracted/refracted, or direct rays. The second arrival occurs at 112.7 seconds, and is comprised of eigenrays that interact with the bottom twice. The third and fourth arrivals occur at 112.7 and 112.9 seconds respectively. Here the number of bottom interactions has increased to three and four bounces. The final arrival occurs at 113.5 seconds and consists of a larger number of eigenrays that interact with the bottom five times. No ray that interacts with the bottom more that this (five times) contributes to a measurable arrival.
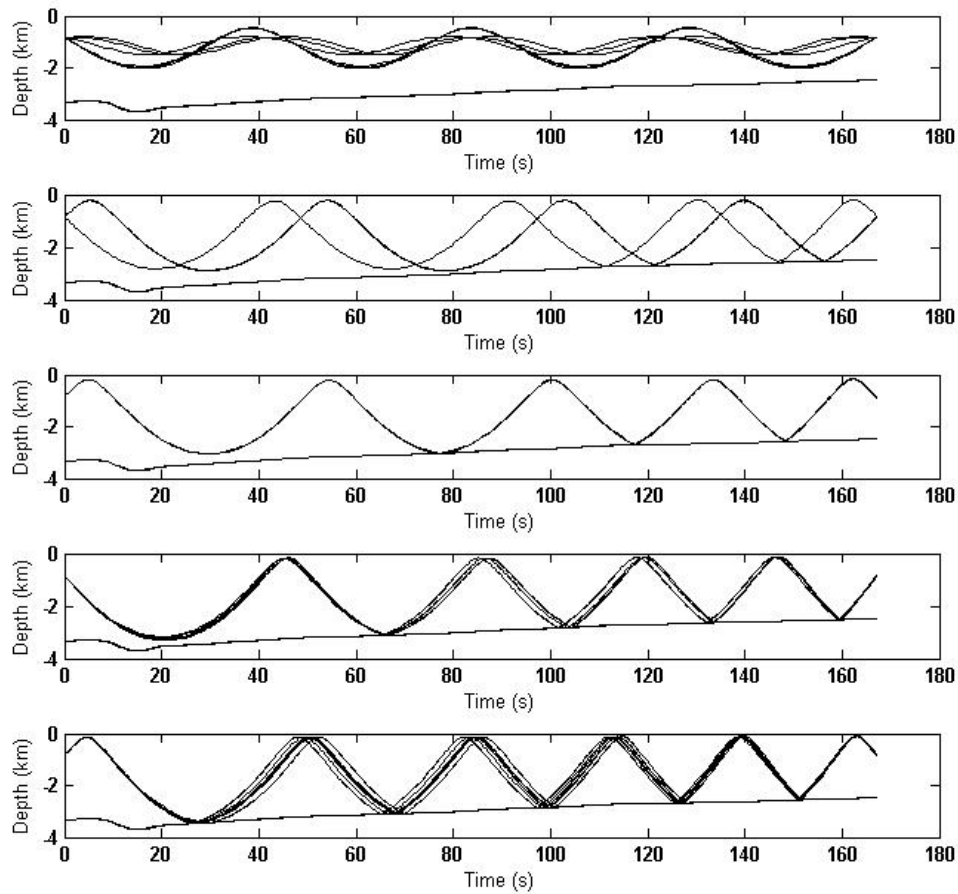
Figure 9. **The modeled eigenray composition for each five of the significant arrivals that were consistently observed during the WISE experiment.**

C.   BOTTOM EVALUATION

1.   Geoacoustic Parameters

The ocean bottom acts as both a reflecting and scattering surface and characterizing its effect on ray amplitude is a complex problem. The bottom composition can vary from rocky to muddy surfaces. Further, even a specific bottom type can vary widely in terms of composition, mean grain size, porosity, etc. Often, there is seasonal variability caused by varying sediment deposition. The bottom can consist of multiple layers of different material, with sound penetrating to a degree based on its frequency and the material in question. The problem is compounded by the fact that in deep water, knowledge of the bottom composition is usually limited to a few core samples. A full discussion of the acoustic properties of the sea floor can be found in (Hamilton 1980).

The HARPO model simulates a reflecting ocean bottom and tracks the bottom and surface interactions. The analysis of the rayset accounts for the amplitude loss and phase change per bottom interaction for a particular eigenray by considering the grazing angle of the ray, the water column sound speed, the sediment sound speed, the density of the bottom, and the attenuation factor $\alpha\, dB/km/Hz$, which represents the attenuation of compression waves by the bottom. Some more sophisticated models differentiate between this attenuation and that of shear waves, but this refinement is not considered in this effort. In general α is determined empirically. Some authors (Urick 1983) have noted that the controlling factor in the acoustic properties seems to be the porosity of the sample, but (Richardson and Briggs 2004) found that the attenuation can depend both on the intrinsic attenuation of the material, and that caused by inhomogeneties in the substance, and thus does not necessarily regress well to porosity. Therefore the values of α utilized in this modeling effort are mainly ones that have been determined from core samples in (Richardson & Briggs 2004) or postulated by (Schneck-Scott 2005).

2.   Alternative Cases

Prior to the conduct of the WISE experiment modeling was conducted as described in (Schneck-Scott 2005) to determine the resolvability of signals in the SCS based on the proposed transmitter and receiver arrangement. Two possible bottom cases

were modeled based on core samples that indicated a bottom that ranged from sand-silt-clay to silty clay. These two possible bottoms were intended to bind the problem as a best and worst case. In (Richardson & Briggs 2004), the authors survey nearly 800 cores from 69 sites around the world in a compilation of physical and acoustic properties. Cases with physical properties in the range of the best and worst case bottoms were selected from this list to add some refinement to the determination. The two cases modeled in (Schneck-Scott 2005) are shown in Table 1. The alternative cases that were examined from (Richardson & Briggs 2004) are shown in Table 2.

Sediment Type	Sand-Silt-Clay Case 1	Silty Clay Case 2
c (m/s)	1600	1521
ρ_{bottom} (kg/km^3)	1.7	1.24
α $(dB/km/Hz)$	.313	.486

Table 1   **Bottom cases modeled in (Schneck-Scott 2005) in preparation for the WISE effort.**

Sediment Type	Clayey Silt Case A	Sand-Silt Case B	Silty clay Case C	Silty Clay Case D	Silty Clay Case E
c (m/s)	1545.5	1614	1507.2	1480.4	1501.7
ρ_{bottom} (kg/km^3)	1.597	1.820	1.313	1.506	1.546
α $(dB/km/Hz)$	0.579	0.462	0.285	0.145	0.166

Table 2   **Alternate bottom cases drawn from (Richardson & Briggs 2004) to provide more refinement in the bottom determination.**

3.   Bottom Characterization

A comparison of the modeled arrival structures generated by the bottoms listed above with the actual arrival structures was conducted. It was possible to immediately reject some of the bottom cases. The arrival structures generated by the original Case 1, and the alternative cases A, and B were extremely inconsistent with the observed arrival structures, containing many high amplitude peaks spread throughout the arrival structure. The structures generated by Cases 2, C, D, and E were much closer to the "lossy" bottom arrival structures that were observed. Results of the comparison of the relative amplitude of the peaks indicated that Case 2, the original worst case postulated by (Schneck-Scott, Sept, 2005) was the closest match to the actual bottom. The alternative structures generated by Cases C, D, and E were in fact too "lossy." The structures generated by these bottoms are shown in Figure 10, where it can be seen that they lack the smaller peaks seen the actual data. Results of the peak-to-peak comparison are summarized in Table 3, for completeness all cases are summarized. The bottom then is determined to be silty-clay bottom characterized as in Table 1, the original Case 2.
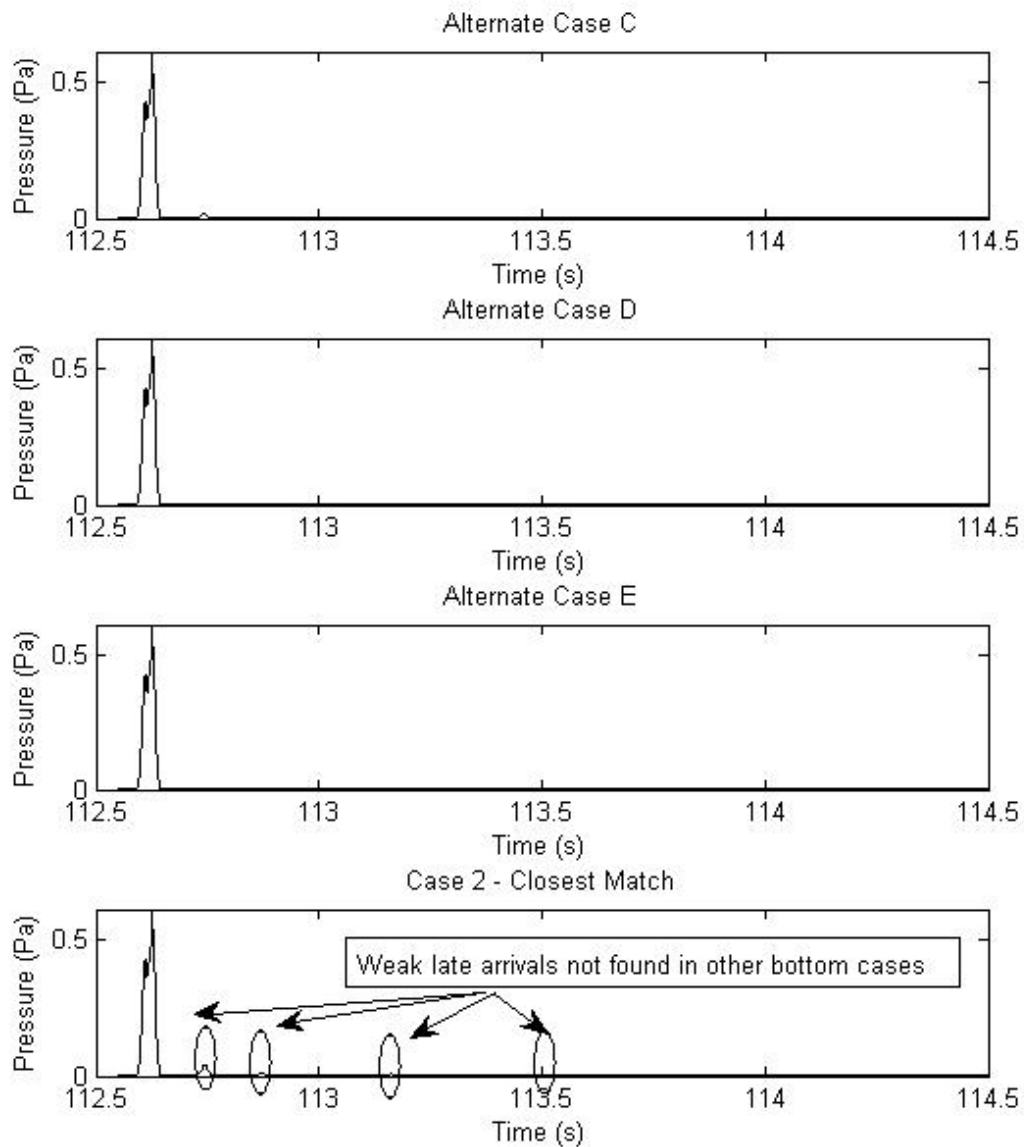
**Figure 10**   The top three panes show the reasonable alternate bottom cases – these cases lack the weak late arrivals that characterize the observed arrival structure. The bottom pane shows Case 2, the case that best matches the observed data

Data Set	2nd Peak	3rd Peak	4th Peak
Actual	~20 dB Down	~30-35 dB Down	~30-38 dB Down
Case 1	~16 dB Down	~25 dB Down	~35 dB Down
Case 2	~24 dB Down	~39 dB Down	~38 dB Down
Case A	~20 dB Down	~30 dB Down	~24 dB Down
Case B	~17 dB Down	~27 dB Down	~17 dB Down
Case C	~30 dB Down	~48 dB Down	~56 dB Down
Case D	~40 dB Down	~60 dB Down	~85 dB Down
Case E	~40 dB Down	~58 dB Down	~65 dB Down

Table 3   Comparisons of the various bottom cases to observed data using peak-to-peak changes on dB scale referenced from the first peak; Case 2 provides the closest match

D.   MODELED ACOUSTIC ARRIVAL STRUCTURE

The modeled arrival structure generated from the silty-clay bottom is shown at 0.001^o resolution in Figure 8. The structure compares favorably with those observed in the WISE experiment, with the peak magnitude well within the observed variability of the observations made during the WISE experiment. The bottom geometry is a dominating factor in the arrival structure. While the initial peak is comprised of refracted/refracted (RR) rays – the subsequent arrivals are comprised of eigenrays that have interacted with the bottom to some extent. It is clear that the vast majority of eigenrays interact with the bottom numerous times. While there are a great number of eigenpaths, only a select few of them actually contribute to a noticeable arrival; this is of course due to the lossy nature of the bottom.

E. MODELED TRANSMISSION LOSS

1. Modeling Transmission Loss

Transmission loss (TL) is an ideal tool for evaluation of acoustic conditions since, as a ratio of energies; it is independent of source strength. Transmission loss is defined as:

$$TL = 10 \log \frac{\int p^2_{\,0}(t)dt}{\int p^2_{\,rcvr}(t)dt} \qquad (3.1)$$

In order to determine a transmission loss curve between the source and receiver, a model arrival structure was generated at 5 km increments, and then numerically integrated in accordance with equation 3.1. This analysis was conducted at a model depth of 400 ft, since that was the depth of the sonobuoy measurements taken.

2. Comparison with Sonobuoy Data

Figure 11 compares the TL model with the sonobuoy data taken during the WISE experiment, expressed as received signal intensity level $(SL - TL)$. While only a few sonobuoy measurements were taken in the region modeled, it appears that they agree very well with the model prediction.
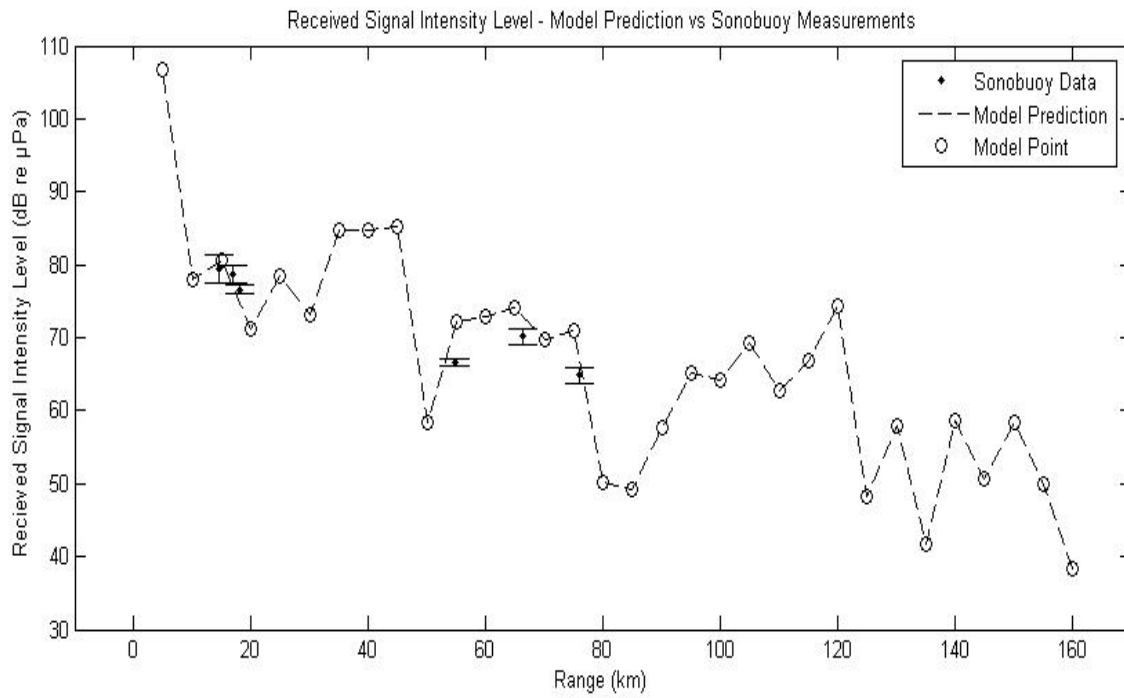
Figure 11. **Comparison of the modeled received level with the sono-buoy received levels observed during the WISE experiment.**

IV. SUMMARY AND CONCLUSIONS

The objective of this thesis was to develop and refine a numerical model of the 400 Hz transmission utilized in the SCS WISE experiment. In particular, it was desired to match the general arrival structure observed during the SCS WISE experiment. This effort utilized a Hamiltonian ray-theory approach and subsequent analysis of the ray set in order to model the acoustic arrival structure generated by a source and receiver in the SCS basin. A mean sound speed profile developed from CTD casts was utilized to create a range-independent sound speed field, which along with accurate bathymetry defined the geometry of the problem. An angular resolution study was conducted to establish convergence of the arrival structure while minimizing computational requirements. The angular aperture for the rays was chosen such that the critical angles for all reasonable bottoms fell within the window utilized. This study established that an angular resolution of 0.005^o provided sufficient resolution to capture all contributing eigenrays and provide a sufficiently convergent estimate of the amplitude loss due to ray tube spreading.

Starting with a general notion of the bottom type (silty-clay), the geo-acoustic properties of the bottom were estimated by generating acoustic arrival structures for a range of bottoms and comparing them with the WISE observations. With both the required angular resolution and the bottom parameters determined, a transmission loss model could be estimated. The predicted TL agreed very well with the sonobuoy measurements that were conducted during the WISE experiment.

Further research will utilize this numerical model to study the multi-scale variability of the acoustic arrival structure, and the impact of trans-basin non-linear waves on acoustic propagation. This future research will attempt to understand the physics of this phenomena and the impact on acoustics in the SCS.

THIS PAGE INTENTIONALLY LEFT BLANK

APPENDIX – DERIVATION OF THE RAY EQUATIONS

A.1 The Ray Equations

In this appendix, a derivation of the ray equations is provided. The approach taken here is that of (Ziomek 1995). A full discussion of the ray approach can be found in (Cornbleet 1983), which discusses the topic through the lens of its close relative, geometric optics. Hamilton's approach is also discussed in that reference, although a simpler approach is found in (Molcho and Censor 1986). A somewhat qualitative description of ray tracing and its limitations can be found in (Urick 1983).

Beginning with the free wave equation and substituting a solution with time harmonic dependence, we obtain the Helmholtz equation, where k_0, is the reference wave number and $k_0 = \dfrac{2\pi f}{c_0}$:

$$
\begin{aligned}
&p(t,\vec{r}) = A(\vec{r})e^{i\omega t} \\
&\Rightarrow \nabla^2 p(\vec{r}) + k_o{}^2 n^2(\vec{r}) p(\vec{r}) = 0 \\
&\text{Where, } n = \frac{c_0}{c(\vec{r})}
\end{aligned}
\tag{A.1}
$$

The further assumption that the solution is comprised of a real amplitude part, and a real phase part, $p(\vec{r}) = A(\vec{r})e^{-ik_0 W(\vec{r})}$, where $W(\vec{r})$ is the eikonal discussed in II.B.1, leads to the transport equation after this solution is substituted into the Helmholtz equation:

$$
[\nabla^2 + k_0{}^2 n^2(\vec{r})]p(\vec{r}) = \nabla^2(A(\vec{r})e^{-ik_0 W(\vec{r})}) + k_0{}^2 n^2(\vec{r})A(\vec{r})e^{-ik_0 W(\vec{r})} = 0
$$

Evaluating this expression with vector identities and equating the real and imaginary parts with zero yields the system:

$$
\begin{aligned}
&\nabla^2 A(\vec{r}) + k_0{}^2 n^2(\vec{r})A(\vec{r}) - k_0{}^2 A(\vec{r})\left|\nabla W(\vec{r})\right|^2 = 0 \\
&2\nabla A(\vec{r}) \cdot \nabla W(\vec{r}) + A(\vec{r})\nabla^2 W(\vec{r}) = 0
\end{aligned}
\tag{A.2}
$$

The second of these equations is the Transport Equation identified in Equation 2.3. The first of these equations can be rewritten as:

$$\frac{\nabla^2 A(\vec{r})}{k_0^2 n^2(\vec{r}) A(\vec{r})} + 1 - \frac{\left|\nabla W(\vec{r})\right|^2}{n^2(\vec{r})} = 0$$

or, equivalently

$$k_0^2 \left|\nabla W(\vec{r})\right|^2 - \frac{\nabla^2 A(\vec{r})}{A(\vec{r})} = n^2(\vec{r})$$

Here we assume that the phase is changing more rapidly than the amplitude, or rather that the change in the amplitude is much less than the change in phase:

$$k_0^2 \left|\nabla W(\vec{r})\right|^2 \gg \left|\frac{\nabla^2 A(\vec{r})}{A(\vec{r})}\right| \tag{A.3}$$

This approximation allows the first equation in (A.2) to be written as:

$$\left|\nabla W(\vec{r})\right|^2 = n^2(\vec{r}) \tag{A.4}$$

This equation is the eikonal equation of (2.3). Recognizing that the inequality (A.3) is equivalent to:

$$\left|\frac{\nabla^2 A(\vec{r})}{k_o^2 A(\vec{r})}\right| \ll 1 \Leftrightarrow 2\pi f \gg \left|\nabla c\right|$$

yields a necessary condition of ray acoustics, one that is satisfied in this modeling effort as discussed in Chapter 2.

In order to derive the ray paths from the eikonal equation, note that the gradient of the eikonal $\nabla W(\vec{r})$ represents the direction of ray propagation. Then, since $\nabla W(\vec{r}) = n(\vec{r})$, and taking the derivative of both sides with respect to s, the arc length along the ray, we obtain:

$$\frac{d}{ds}\nabla W(\vec{r}) = \nabla n(\vec{r}) = \frac{d}{ds}(n(\vec{r})\frac{d\vec{r}}{ds}) \tag{A.5}$$

This coupled set of ordinary differential equations can then be solved to obtain the ray paths.

A.2 The Hamiltonian

HARPO calculates ray paths by integrating Hamilton's equations. In general the Hamiltonian, H is defined to be zero along ray paths, and is the dispersion relation of the acoustic waves set equal to zero:

$$H(\vec{r},\vec{k}) = [\omega - \vec{k} \cdot u(\vec{r})]^2 - c^2(\vec{r})k^2 \tag{A.6}$$

Here, $\omega = 2\pi f$, $u(\vec{r})$ is the current field, $c(\vec{r})$ is the sound speed, and k is the wave number. In this modeling effort, a static (or currentless) ocean is simulated and (A.6) reduces to:

$$H = \omega^2 - c^2(\vec{r})k^2 \tag{A.7}$$

Physically, the quantity $\dfrac{d\omega}{dk}$ is the group velocity and represents the speed at which energy propagates for the waves. Since HARPO utilizes polar-spherical coordinates the form of the (A.7) utilized is, as noted in (Georges, Jones, & Riley, 1986):

$$H = \omega^2 - (k_r^2 + k_\theta^2 + k_\phi^2)c^2(t,r,\theta,\phi) = 0 \tag{A.8}$$

In order to obtain the system of ordinary differential equations, the partial derivatives of H are taken with respect to each of $t,r,\theta,\phi,k_r,k_\theta,k_\phi$. This yields the system of equations (Georges, Jones, & Riley, 1986) that is actually numerically integrated:

33

$$\frac{\partial H}{\partial t} = -k^2 \frac{\partial c^2}{\partial t}$$

$$\frac{\partial H}{\partial r} = -k^2 \frac{\partial c^2}{\partial r}$$

$$\frac{\partial H}{\partial \theta} = -k^2 \frac{\partial c^2}{\partial \theta}$$

$$\frac{\partial H}{\partial \phi} = -k^2 \frac{\partial c^2}{\partial \phi}$$

$$\frac{\partial H}{\partial \omega} = 2\omega$$

$$\frac{\partial H}{\partial k_r} = -2c^2 k_r$$

$$\frac{\partial H}{\partial k_\theta} = -2c^2 k_\theta$$

$$\frac{\partial H}{\partial k_\phi} = -2c^2 k_\phi$$

$$\vec{k} \bullet \frac{\partial H}{\partial \vec{k}} = -2c^2 k^2$$

LIST OF REFERENCES

Chiu, C. et al. "Observed acoustic arrival structure and intensity variability induced by transbasin nonlinear internal waves in the South China Sea basin." *J. Acoust. Soc. Am.* 123, no. 5, pg 3588 (2008).

Chiu, C.S., A.J. Semtner, C.M. Ort, J.H. Miller, and L.L. Ehret. "A ray variability analysis of sound transmission from Heard Island to California." *J. Acoust. Soc. Am.* 96, no. 4 (October 1994).

Clay, C.S., and H. Medwin. *Acoustic oceanography.* New York: John Wiley and Sons, 1977.

Cornbleet, Sidney. "Geometrical Optics Reviewed: A New Light on an Old Subject." *Proceedings of the IEEE* 71, no. 4 (April 1983).

Georges, T.M., R. Michael Jones, and J.P. Riley. "Simulating Ocean Acoustic Tomography Measurements with Hamiltonian Ray Tracing." *IEEE Journal of Oceanic Engineering* OE-11, no. 1 (1986).

Hager, C.A. "Assesment of the Performance of the Near-Bottom Hydrophones of the U.S. Navy Southern California Offshore Range in Detecting, Localizing, and Reconstructing 10-20 kHz Odontocete Whistles." *PHD Thesis, Naval Postgraduate School*, March 2008.

Hamilton, E. L. "Geoacoustic modeling of the sea floor." *J. Acoust. Soc. Am.* 68, no. 5 (1980).

Jones, R.M, J.P. Riley, and T.M. Georges. *HARPO: A Versatile Three-Dimensional Hamiltonian Ray-Tracing Program for Acoustic Waves in an Ocean with Irregular Bottom.* Boulder, CO: Wave Propagation Laboratory, National Ocean and Atmospheric Administration, 1986.

Liu, C. S., S. Y. Liu, S. E. Lallemand, N. Lundberg, and D. Reed. "Digital Elevation Model Offshore Taiwan and Its Tectonic Implications." *Terrestrial, Atmospheric and Oceanic Sciences* 9, no. 4 (1998): 705-73 8.

Miller, Christopher W., Marla Stone, Keith Wyckoff, Ching-Sang Chiu, and Steve Ramp. *Preliminary results from the Windy Island Soliton Experiment (WISE) Acoustics Moorings.* Naval Postgraduate School, 2009.

Molcho, Jonathon, and Dan Censor. "A simple derivation and an example of Hamiltonian ray propogation." *Am. J. Phys.* 54, no. 4 (1986): 351-353.

Ramp, S.R. et al. "Internal Solitons in the Northeastern South China Sea Part I: Sources and Deep Water Propogation." *IEEE J. Oceanic Engineering* 29 (October 2004).

Richardson, M.D., and K.B. Briggs. "Relationship Among Sediment Physical and Acoustic Properties in Siliciclastic and Carbonate Sediments." *Proceedings of the Seventh European Conference on Underwater Acoustics, ECUA 2004.* Delft, The Netherlands, 5-8 July 2004.

Schneck-Scott, A. "Detection and Resolvability of Pulsed Acoustic Signals Through the South China Sea basin: A Modeling Analysis." *Master's Thesis, Naval Postgraduate School*, September 2005.

Urick, R.J. *Principles of Underwater Sound.* Los Altos Hills, Ca: Peninsula Publishing, 1983.

Ziomek, L.J. *Fundamentals of Acoustic Field Theory and Space-Time Signal Processing.* Boca Raton, FL: CRC Press , 1995.

INITIAL DISTRIBUTION LIST

1. Defense Technical Information Center
   Ft. Belvoir, Virginia

2. Dudley Knox Library
   Naval Postgraduate School
   Monterey, California

3. Dr. Clyde Scandrett
   Naval Postgraduate School
   Monterey, California

4. Dr. Ching-Sang Chiu
   Naval Postgraduate School
   Monterey, California

5. CDR Ben Reeder
   Office of Naval Research
   Washington, DC